GALILEO DISPOSAL ORBIT STRATEGY: RESONANCES, CHAOS, AND STABILITY

Aaron J. Rosengren(1), Jérôme Daquin(2), Elisa Maria Alessi(3), Giovanni B. Valsecchi(4), Alessandro Rossi(5), and Florent Deleflie(6)

(1)(3)(4)(5)*IFAC-CNR, Via Madonna del Piano 10, 50019 Sesto Fiorentino (FI), Italy, +39 055 5226315, a.rosengren@ifac.cnr.it*

(2)*Thales Services, 3 Impasse de l'Europe, 31400 Toulouse, France, +33 5 62 88 85 06, jerome.daquin@imcce.fr*

(4)*IAPS-INAF, Via Fosso del Cavaliere 100, 00133 Roma, Italy, +39 06 4993 4446, giovanni@iaps.inaf.it*

(2)(6)*IMCCE/Observatoire de Paris - Université Lille1, 1 Impasse de l'Observatoire, 59000 Lille, France, +33 1 40 51 22 74, florent.deleflie@imcce.fr*

Abstract:

Recent studies have shown that the Global Navigation Satellite Systems exist in a background of complex resonant phenomena and chaotic motion. Woven throughout the inclination and eccentricity phase space is an exceedingly complicated web-like structure of lunisolar secular resonances, which become particularly dense near the inclinations of the navigation satellite orbits. As in all cases in the Solar System, chaos emerges from the interaction and overlapping of neighboring resonances. The precarious state of the four navigation constellations, perched on the threshold of instability, makes it understandable why all past efforts to define stable graveyard orbits, especially in the case of Galileo, were bound to fail; the region is far too complex to allow of an adoption of the simple geosynchronous disposal strategy. We retrace one such recent attempt, funded by ESA's General Studies Programme in the frame of the GreenOPS initiative, that uses a systematic parametric approach and the straightforward maximum-eccentricity method to identify long-term stable regions, suitable for robust graveyards, as well as large-scale excursions in eccentricity, which can be used for post-mission deorbiting of constellation satellites. We then apply our new results on the stunningly rich dynamical structure of the MEO region toward the analysis of these disposal strategies for Galileo, and discuss the practical implications for chaos in this regime.

Keywords: *Medium-Earth Orbits, Chaos, Resonances, Fast Lyapunov Indicator, Stability Maps.*

1. Introduction

The application of the mathematical tools and techniques of nonlinear dynamics has provided astronomers with a deeper understanding of the dynamical processes that have helped to shape the Solar System [1]. Resonant phenomena connected with the commensurability of frequencies of interacting motions abound in celestial mechanics and have both dynamical and theoretical importance. A succession of remarkable features in the asteroid belt, known as the Kirkwood gaps, vividly illustrates the physical significance of resonances and chaos in real systems. Considerable impetus was imparted over the past three decades to the study and understanding of this type of chaotic unpredictability and its manifestation in other astronomical problems.

With chaotic motions being a natural consequence of even the most simplest of systems, it may no longer be sensible to investigate the "exact" trajectory of a celestial body (natural or artificial) in a given time interval [2]. Far beyond the Lyapunov time, the characteristic time over which an orbit is said to remain predictable, it is not possible to reproduce the same time evolution if the system is chaotic, due to the exponential growth of uncertainties (in the initial state, mis-modeling effects, numerical errors, etc.). The irregular and haphazard character of the chaotic path of a celestial body reflects a similar irregularity in the trajectories of stochastic systems, as if the former were influenced by a random perturbation even though, in fact, the motion is governed by purely deterministic dynamical equations. There is, however, an essential difference: "classical (that is, non-quantum mechanical) chaotic systems are not in any sense intrinsically random or unpredictable," as John Barrow puts it, "they merely possess extreme sensitivity to ignorance [3]." Despite the unpredictability of the path of a particular orbit, chaotic systems can exhibit statistical regularities, and have stable, predictable, long-term, average behaviors [4]. The lesson is that the time evolution of a chaotic system can only be described in statistical terms; one must study the statistical properties of ensembles of stochastic orbits [2, 5].

Our knowledge about the stability of the orbits of artificial satellites is still incomplete. Despite over fifty years of space activities, we know amazingly little about the dynamical environment occupied by artificial satellites and space debris. Strange as it may seem, we understand the structure and evolution of the, mostly invisible, trans-Neptunian belts of small bodies [1] far better than we understand that of the artificial bodies that orbit our terrestrial abode. Before these remnants of Solar-System formation diverted the interests and energies of space-age astronomers, such astrodynamical problems stood in the foremost rank of astronomical research work [6]. The kind of Newtonian determinism brought to bear during the 1960s has continued merrily along in astrodynamics, unheeding the fundamental discoveries of nonlinear dynamics. Today we take for granted the great power and scope of modern computers, treating them as the supreme intelligence imagined by Laplace, and the construction of increasingly more 'accurate' and grandiloquent dynamical models and simulation capabilities has become the central task of the field.

As long as our thought processes are limited along the inflexibilities of determinism, we will remain forever ignorant of the possible range and vagaries of chaos in Earth satellite orbits. An understanding of these chaotic phenomena is of fundamental importance for all efforts to assess debris mitigation measures — efforts which may shed much light on the design and definition of optimal disposal strategies throughout all space regions (LEO, MEO, GEO, HEO, LPO), taking into account orbital interaction and environmental evolution. In this context, there has been considerable recent interest in designing novel de-orbiting or re-orbiting solutions for the MEO navigation satellites [7, 8, 9], since the operational constellations and recommended graveyard orbits have been found to be unstable [10].

The intent of this paper is to provide a case study on the European Galileo system that can be used as a reference for the other constellations, and to serve as a springboard for investigating new dynamical situations that may arise. We begin with a parametric numerical study on two end-of-life disposal strategies, based on the Laplacian paradigm, which investigates the role of the initial parameters of the disposal orbits (the semi-major axis, eccentricity, inclination, orientation phase angles, and epoch) on their long-term stability over centennial and longer timescales. We summarize our findings from this extensive numerical experiment and show, based on our recent studies of the dynamical structure of MEO [11], why such general recommendations and guidelines should be taken with a grain of salt. We then tailor our results on the resonant and chaotic structures of the phase space near lunisolar secular resonances [11, 12] towards the analysis of the disposal options for Galileo. We omit on this occasion any mathematical discussion and simply present the main results at which we have arrived.

2. Parametric Study on Two Disposal Strategies

2.1. Introduction and Experimental Setup

Considerable attention is now being devoted to the problem of determining the long-term stability of medium-Earth orbits. The problem has been especially timely ever since the advent and launch of the European Galileo and the Chinese Beidou constellations. The main physical mechanisms that can lead to substantial variations in eccentricity, thereby affecting the perigee radius, are resonance phenomena associated with the orbital motion of artificial satellites. While the dynamics of MEOs, governed mainly by the inhomogeneous, non-spherical gravitational field of the Earth, is usually only weakly disturbed by lunar and solar gravitational perturbations, for certain initial conditions, appreciable effects can build up through accumulation over long periods of time. Such lunisolar resonances, which can drastically alter the satellite's orbital lifetime, generally occur when the second harmonic of the Earth's gravitational potential (J_2) causes nodal and apsidal motions which preserve a favorable relative orientation between the orbit and the direction of the disturbing force [12]. There is also another class of resonances that occurs when the satellite's mean motion is commensurable with the Earth's rotation rate, thereby enhancing the perturbing effects of specific tesseral harmonics in the geopotential. These tesseral resonances pervade the MEOs of the navigation satellites [7] and their net effects are to produce small, localized instabilities in the semi-major axis.

A proper understanding of the stability characteristics of the two main types of resonances in MEO is vital for the analysis and design of disposal strategies for the four constellations. This concerns particularly the question as to whether suitable stable orbits exist such that satellites in these graveyards will not interfere with the constellations, or whether strong instabilities exist, whose destabilizing effects manifest themselves on decadal to centennial timescales, that can be exploited to permanently clear this region of space from any future collision hazard. The process of dynamical clearing of resonant orbits is a new paradigm in post-mission disposal, but has not been hitherto rigorously studied.

Accordingly, in the framework of the ESA/GSP Contract No. 4000107201/12/F/MOS, we investigate the structure of the web of commensurabilities in the MEO region, using a dynamical model accounting for the Earth's gravity field, lunisolar perturbations, and solar radiation pressure (Tab. 1). We study particularly to what extent the change in initial parameters of storage orbits can affect the long-term stability of these orbits over long intervals of time. This study is based on the numerical integration of the averaged equations of motion, using a semi-analytic model suitable for all dynamical configurations, which has been approved as the reference model for the French Space Operations Act (through the software, STELA, and its fortran prototype[1]).

[1]STELA (Semi-analytic Tool for End of Life Analysis) can be downloaded from the CNES website:

Table 1. Gravitational perturbations added to the central part of the geopotential for the numerical stability analysis. Model 4 (which also includes SRP perturbations with Earth shadow effects) is used for the MEM maps of the ESA study and model 1 for the FLI and Lyapunov time stability maps of Section 4.

	ZONAL	TESSERAL	LUNAR	SOLAR
model 1	J_2	not considered	up to degree 2	up to degree 2
model 2	$J_2, J_2^2, J_3 \cdots, J_5$	not considered	up to degree 4	up to degree 3
model 3	$J_2, J_2^2, J_3 \cdots, J_5$	up to degree & order 5	up to degree 4	up to degree 3
model 4	$J_2, J_2^2, J_3 \cdots, J_7$	up to degree & order 5	up to degree 3	up to degree 3
model 5	$J_2, J_2^2, J_3 \cdots, J_7$	up to degree & order 5	up to degree 4	up to degree 3

An analysis of the historical practices of the GNSS constellations was performed in order to properly define the reference simulation scenario [7]. The nominal initial conditions and values of area-to-mass ratio considered for each disposal strategy are displayed in Tab. 2. For the *graveyard orbit scenario*, it is important to ensure that the storage orbits have only small-amplitude orbital deformations over long periods of time, so that the inactive satellites cannot cross the orbital region of active GNSS components (and possibly collide). This in turn implies that we must minimize the long-term eccentricity growth in order to delay or prevent the penetration of the GNSS altitude shells. Alternatively, for the *eccentricity growth scenario*[2], we explore the possibility of de-orbiting satellites by pushing them into unstable phase-space regions that would slowly decrease their perigee distances, leading to a long-term reduction in the combined constellation and intra-graveyard collision risks.

The numerical investigation consisted in propagating the initial conditions of Tab. 2 for 200 years, under the dynamical model 4 in Tab. 1, for a large variety of initial orientation phase parameters and analyzing the maximum eccentricity attained in each case. This maximum-eccentricity method (MEM) provides a straightforward indication of 'stability' and has been used in a number of astronomical contexts [13, 14, 15]. Instinctively and historically, we expect that the orbits become more unstable as their eccentricities grow; yet, we note that this method is not necessarily an estimator of chaos and stability (since large amplitude variations of eccentricity could be due to regular motion, e.g., secular perturbations; and small oscillations could be the result of slow manifestations of chaotic behaviors, e.g., orbits with large Lyapunov times). We characterize each initial point of the parameter plane by their maximum eccentricity value (or a closely related quantity) under the following conditions:

1. 36 equally spaced values of $\omega \in [0^\circ : 360^\circ]$ in increments of 10°;
2. 36 equally spaced values of $\Omega \in [0^\circ : 360^\circ]$ in increments of 10°;
3. 38 equally spaced initial epochs t_0.

http://logiciels.cnes.fr/STELA/en/logiciel.htm

[2]Note that for this disposal strategy, a maneuver ($\Delta v \sim 100$ m/s) is applied at the nominal orbit of the Galileo constellation; i.e., at the same initial orbital elements as in the graveyard case, except for the semi-major axis which is lowered by $\Delta a = 550$ km, resulting in the semi-major axis and eccentricity displayed in the second row of Tab. 2.

The same analysis has also been performed by increasing and decreasing, respectively, the initial inclination by 1° with respect to the nominal value. The aim is not only to see if the known resonant harmonic $2\omega+\Omega$ is actually the most significant, as suggested, justly or unjustly, by many others [10, 9], but also to gain insight on the role of the initial inclination and of the Earth-Moon-Sun dynamical configuration on the evolution of the orbits.

Table 2. Initial mean orbital elements considered for the disposal orbits of the Galileo constellations, and the corresponding values of area and mass. The difference in semi-major axis Δa with respect to the nominal constellation is also shown.

Disposal Strategy	a (km)	Δa (km)	e	i (deg)	A (m^2)	m (kg)
Graveyard Orbit	30,150	550	0.001	56	9.3	665
Eccentricity Growth	28,086	-1514	0.0539	56	9.3	665

The Saros Cycle and Earth's Orbital Environment : Any account of motion in the Earth-Moon-Sun system has to start with a description of the dynamical configuration of this three-body problem. The motion of the Moon manifests an abundance of irregularities, many of them large enough to have been discovered by ancient astronomers. While the Moon's actual motion is very complex, Perozzi and colleagues [16] have shown through the use of eclipse records and the refined lunar ephemeris computed at JPL, which accounts for all Solar System perturbations, that the relative dynamical geometry of the Earth-Moon-Sun system at any time is very nearly repeated after a period of time equal in length to the classical cycle known as the Saros[3]. Saros means repetition and indicates a period of 6 585.321 347 days, after which the Sun has returned to the same place it occupied with respect to the nodes of the Moon's orbit when the cycle began. As a consequence, the geocentric lunar orbit is nearly periodic with such period.

Armed with the above knowledge, we have made our numerical integrations also with the purpose of investigating whether after every Saros a specific configuration of (Ω,ω) leads to the same eccentricity growth. To this end, the simulations were performed every $\Delta t = \text{Saros}/19 \approx 346.59586$ days, starting from $t_0 = 26$ February 1998 (a solar eclipse epoch) to $t_f = 2$ Saros. We have chosen this time step because it corresponds to an eclipse year, the period of time after which the Moon passes through the same node and the Earth, Moon, and Sun are aligned.

2.2. Simulation Results and Discussion

We present here only a subset of our results as the full scope of this study will be given in a later paper and its relation to the other navigation constellations will be formulated there more completely. No space will be devoted therefore to any comparison between the similar, albeit less systematic, efforts to tackle this problem by other groups of researchers [8, 9].

[3]The Saros has been the basis for which predicting eclipses rests since the very dawn of Chaldean history; after the lapse of the Saros period of roughly 6585 days, solar and lunar eclipses recur under almost identical circumstances except that they are displaced about 120° westward on the Earth. The near repetition of eclipses is a consequence of the set of near commensurabilities existing between the various types of lunar months; namely, 223 synodic months is nearly 239 anomalistic months and 242 draconic months.

Figure 1 shows a sample of results from this experiment, and Fig. 2 outlines an ω–targeting strategy to achieve the desired outcome. Similar MEM maps were made for each eclipse year, and the variations in inclination and semi-major axis were tracked in addition to the eccentricity[4], from which we can make the following general observations. The semi-major axis does not change significantly in 200 years (at most 70 km in absolute value) in any of the cases explored. Consequently, to avoid interferences with the operational constellation, the eccentricity should not exceed 0.02. The minimum eccentricity required to re-enter the atmosphere, assumed to occur whenever the altitude reaches at least 120 km, is about 0.77. The near invariability of the semi-major axis leads us to conclude that the tesseral harmonics cannot be responsible for the noted eccentricity instabilities.

For the *graveyard orbit* scenario, we noticed that the eccentricity can grow up to about 0.4, for any of the considered initial inclinations. Moreover, we note the vertical bands of stability (negligible eccentricity growth) in (Ω, ω), Fig. 1, which shift as a function of t_0 (not shown here). In general, we found that it was nearly always possible to target an argument of perigee ensuring 'stability' (Fig. 2); that is, for any given (t_0, Ω) there exists at least one initial ω corresponding to a safe disposal. The situation seems more favorable if the initial inclination is increased by 1°, in the sense that the stable vertical bands are wider.

Concerning the *eccentricity growth* scenario, we found that the eccentricity can increase by up to 0.8, for the three initial values of inclination considered. In the nominal Galileo case, the eccentricity growth is remarkable in the entire (t_0, Ω, ω) phase space; specifically, for any given epoch and ascending node, there exits always one (but generally more) initial ω leading to a re-entry (Fig. 2). In the -1° case, re-entry values for e can be achieved if $\Omega \in [50^\circ, 300^\circ]$, while in the $+1^\circ$ case, the Ω range depends on t_0. If the satellite's node does not match these such values, then the eccentricity tends to stay below 0.1. Atmospheric re-entries were found for the three cases to occur only after at least 100 years.

Finally, we observed a very interesting characteristic of this multi-frequency and highly-perturbed dynamical system. We have performed further analysis with respect to the behavior in time of the maps, by simulating the eccentricity evolution starting from initial epochs displaced by 5 Saros periods from the first 19 considered eclipse year epochs. This revealed that the MEM maps are not periodic over the Saros cycle (~ 18.03 years), but in fact over 1 nodal regression period of the Moon (~ 18.61 years). At first sight, this seems rather surprising, but when duly considered, manifests itself as a natural consequence of the lunar perturbing force, which we now speculate as the main driver of the long-term dynamics. First noted by Musen [17], when doubly averaged, the long-period lunar effect "depends only upon the position of the orbital plane of the Moon and is not influenced by the position of the lunar perigee." Thus, we should not expect the general behavior to be periodic over the Saros period, which intrinsically accounts for both the nodal regression and apsidal precession.

[4]The inclination behavior will not be discussed here.

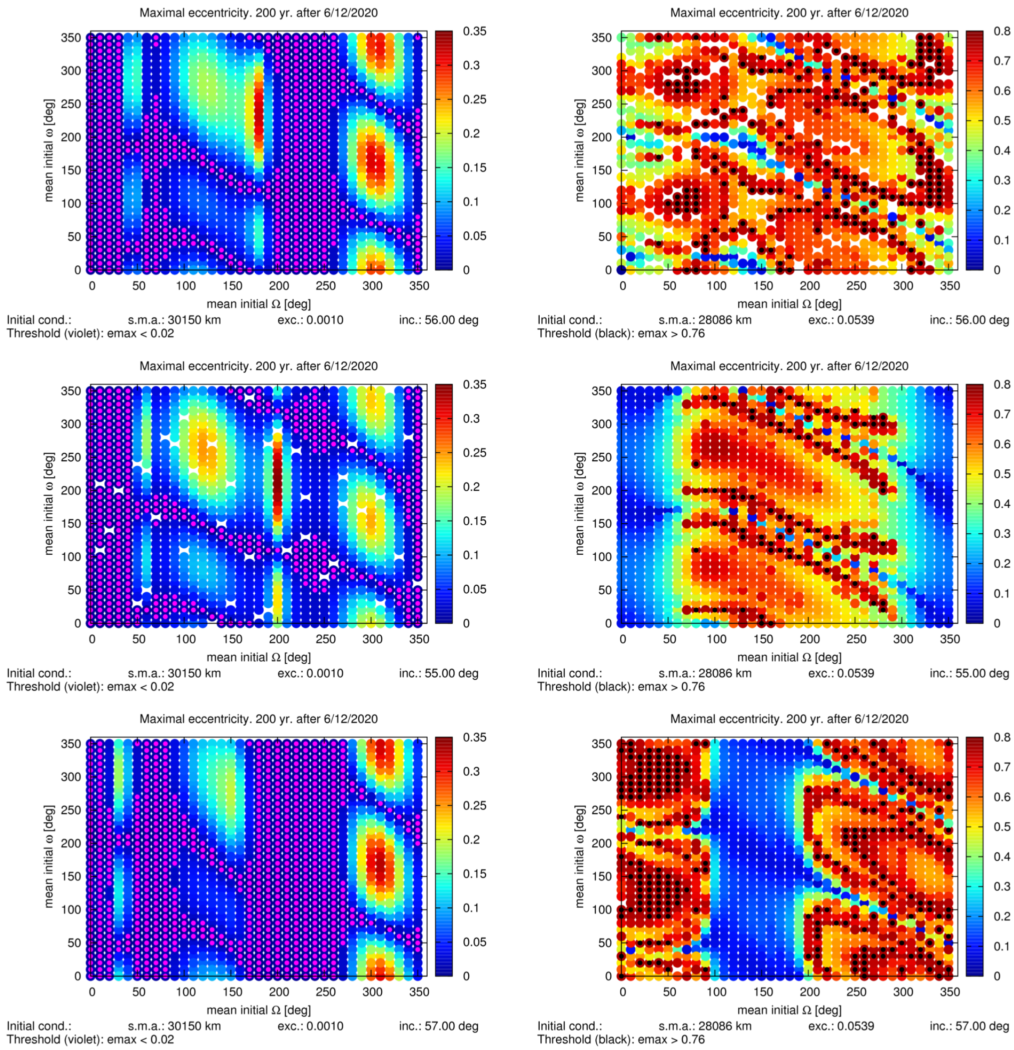

Figure 1. The maximum eccentricity attained in 200 years (colorbar), as a function of the initial longitude of ascending node and argument of perigee, at a given epoch, for the graveyard orbit (left) and eccentricity growth (right) scenarios. Points that meet the various thresholds are indicated by violet ($e_{\max} < 0.02$) and black ($e_{\max} > 0.76$), and the empty white spaces are locations where data is missing due to numerical issues.

Practical Implications of Chaos : Any initial uncertainty in our knowledge of a chaotic system will have small consequences early but profound consequences late, often being rapidly amplified in time. While it is true that the verification of some criteria of stability to define the initial parameters of storage orbits requires long-term orbit propagation up to more than 100 years, most international guidelines and recommendations seem fixated on 200-year forecasts. The 200-year timespan for future projections is not only arbitrary, but completely nonsensical from a dynamical perspective. Every distinct problem in orbital dynamics conditions its own particular scheme of computation, and the question of an appropriate timescale upon which to investigate cannot therefore be answered in a general manner; the answer depends largely on the problem in question and on the degree of knowledge aimed at. An improper assessment can lead to erroneous conclusions regarding stability

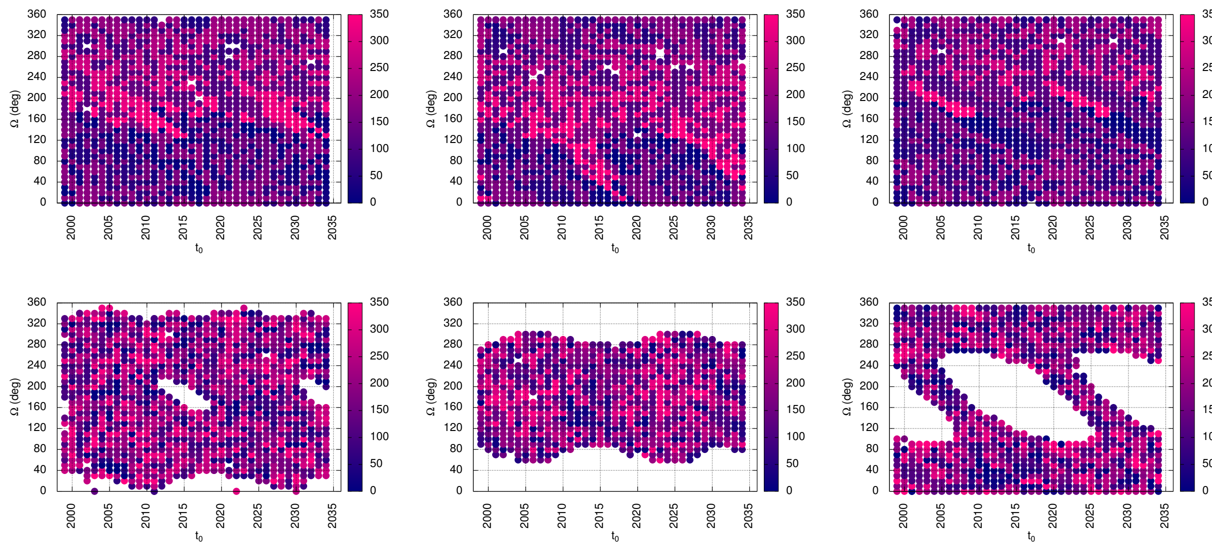

Figure 2. The ω–targeting strategy: the value of argument of perigee (colorbar) which ensures that the eccentricity will not exceed 0.02 in 200 years (top) or which ensures a re-entry (bottom), as a function of the initial epoch and longitude of ascending node. Left: nominal initial inclination; middle: initial inclination decreased by 1°; right: initial inclination increased by 1°.

and chaos. Consider, for example, one of the declared safe graveyard orbits of Fig. 1, as shown in Fig. 3. This orbit does not manifest any significant eccentricity growth for 200 years, and yet is revealed by our stability analysis to be chaotic with a Lyapunov time of 55 years. Alternatively, chaotic orbits which initially appear to re-enter may follow evolutionary paths that lead to long-lasting eccentric orbits (Fig. 3(b)).

3. Resonance Overlap and the Origin of Chaos

3.1. Background

Resonances are regions in the phase space of a dynamical system in which the frequencies of some angular variables become nearly commensurate. Such regions have a profound effect on the long-term dynamics of the system, giving rise to a rich spectrum of highly complicated behaviors [4]. It is of great practical importance to understand the mechanisms behind these irregular features, both qualitatively and quantitatively. Recently, it has been realized that lunisolar secular resonances (i.e., caused by the Moon and the Sun on long timescales) are of particular importance in the medium-Earth orbit regime [12, 11]. We review in this section our investigations on the detection of regular structures and chaotic behaviors in the phase space near the navigation satellites. Studying the long-term effects of lunisolar secular resonances is crucial, not only because we need to understand their stability properties, but also because we would like to know whether they could be used (and how) for eventually deorbiting satellites, by forcing them to slowly drift towards high eccentricities and different inclinations.

Despite the variety and complexity of the nature of the dynamics near resonances, we can build an

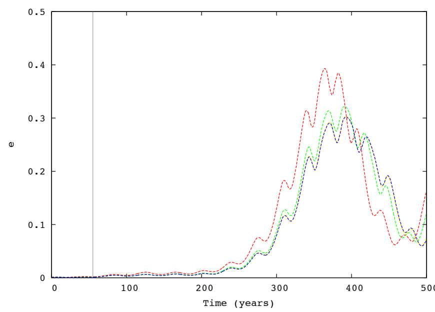

(a) A stable case. $a_0 = 30,150$ km, $e_0 = 0.001$, $i_0 = 56°$, $\Omega_0 = 70°$, $\omega_0 = 70°$, epoch: 6 DEC 2020.

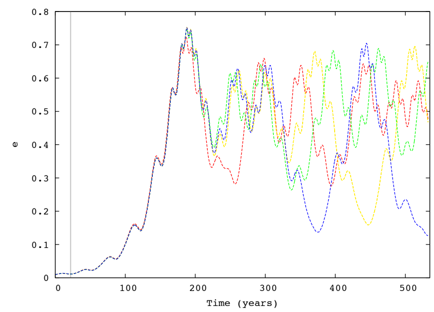

(b) An unstable case. $a_0 = 29,600$ km, $e_0 = 0.01$, $i_0 = 55°$, $\Omega_0 = 120°$, $\omega_0 = 30°$, epoch: 2 MAR 1969.

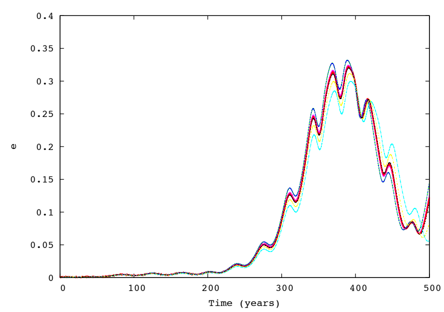

(c) Integrations of nearby orbits with uncertainties in e_0 of 10%, 5%, and 1%. The thick red line is the nominal orbit of 3(a).

Figure 3. Numerical ensemble integrations according to the various dynamical models (top) in Tab. 1 and of nearby orbits (bottom) for apparently safe disposal and re-entry orbits. The vertical lines indicate the Lyapunov times, corresponding to an average limit of predictability of each orbit.

intuitive understanding using the mechanics of a pendulum. Pendulum-like behavior is fundamental to the mathematics of resonance: phase-space structure, separatrices of a periodic motion, and stability. The principal effect of the interaction of two resonances is to produce qualitative changes in the separatrix of the perturbed resonance, producing a stochastic layer in its vicinity. The onset of deterministic chaos and the loss of stability is predicted to occur when the separation between the resonances is of the order of their resonance widths [4]. Nearly all chaos in the Solar System and beyond has been attributed to the overlapping of resonances [1][5].

3.2. Lunisolar Resonant Skeleton

Focusing on the MEO region located between three and five Earth radii, namely in a region for which the variation of the argument of perigee ω and longitude of ascending node Ω may be estimated by considering only the effect of J_2 (the second zonal harmonic coefficient of the geopotential) and for which the lunar and solar potentials may be approximated with sufficient accuracy by quadrupole fields, the center of each lunisolar secular resonances (for prograde orbits) may be defined in the

[5] Note that while this is the main physical mechanism for the generation of chaos, two overlapping resonances may lead to regular motion sometimes; see, e.g., [18].

inclination–eccentricity (i–e) phase space by the curves [12, 11]

$$\mathscr{C}_{\boldsymbol{n}} = \Big\{(i,e) \in [0,\frac{\pi}{2}] \times [0,1] \;:\; \psi_{\boldsymbol{n}} = n_1\dot{\omega} + n_2\dot{\Omega} + n_3\dot{\Omega}_{\mathrm{M}} = 0\Big\} \tag{1}$$

for $n_1 = \{-2,0,2\}$, $n_2 = \{0,1,2\}$, $n_3 \in [-2,2]$, where

$$\dot{\omega}(i,e) = \frac{3}{4}\frac{J_2R^2\sqrt{\mu}}{a^{7/2}}\frac{5\cos^2 i - 1}{(1-e^2)^2}, \quad \dot{\Omega}(i,e) = -\frac{3}{2}\frac{J_2R^2\sqrt{\mu}}{a^{7/2}}\frac{\cos i}{(1-e^2)^2}, \quad \dot{\Omega}_M = -0.053^\circ/\text{day}. \tag{2}$$

Here the semi-major axis a is a parameter[6], R is the mean equatorial radius of the Earth and μ its gravitational parameter. Using the full machinery for pendulums, it can be shown that the curves delimiting the maximum separatrix width of each resonance (i.e., the maximum amplitude inside the libration zone) are defined by [11]

$$\mathscr{W}_{\boldsymbol{n}}^{\pm} \equiv \Big\{(i,e) \in [0,\frac{\pi}{2}] \times [0,1] \;:\; \dot{\psi}_{\boldsymbol{n}} = \pm\Delta_{\boldsymbol{n}}\Big\}, \tag{3}$$

in which

$$\Delta_{\boldsymbol{n}} = 2\sqrt{\frac{3}{2}\frac{J_2R^2}{a^4}\left|\frac{n_1^2(2-15\cos^2 i_\star) + 10 n_1 n_2 \cos i_\star - n_2^2}{(1-e_\star^2)^{5/2}} h_{\boldsymbol{n}}(i_\star, e_\star)\right|}, \tag{4}$$

where $h_{\boldsymbol{n}}$ is the harmonic coefficient in the lunar and solar disturbing function expansions, associated with the harmonic angle which is in resonance[7], and $(i_\star, e_\star)$ are the 'actions' at exact resonance; namely, the inclinations and eccentricities that satisfy (1).

Figure 4 shows that resonances fill the phase-space near the Galileo constellation. These resonances form in some sense the skeleton or dynamical backbone, organizing and governing the long-term orbital motion. The resulting dynamics can be quite complex, and it has been shown that chaos ensues where resonances overlap [12]. It is particularly noteworthy that the nominal inclination of Galileo lies right at the cusp of three distinct and dynamically significant resonant harmonics. Such naivety in the placement of these important assists reflects the need of a real dynamical assessment in constellation design. What is more to the point is that the conclusions drawn from the computationally expensive parametric study of Section 2. are easily corroborated here. In the graveyard orbit scenario, increasing the inclination by 1° moves the storage orbits outside of the overlapping regime, and thus we would naturally expect this to be the more dynamically stable case. For the eccentricity growth scenario, the nominal Galileo case is the more unstable situation because the orbits lie at the primary $\psi_{2,1,0}$ resonance, while the instabilities in the other inclination cases are likely due to the generation of secondary resonances (commensurabilities of the libration and circulation frequencies of primary resonances) that expand the size of the chaotic zones about the $\dot{\psi}_{2,1,0}$ resonance. Rather ironically, the targeting of a lower semi-major axis for this disposal strategy appears inappropriate, as keeping the constellation at the Galileo semi-major axis would have resulted in greater instabilities with the interaction of the three distinct primary resonances.

[6]The lunar and solar perturbation parameters are proportional to a as $\varepsilon_{\mathrm{M}} = \varepsilon_{\mathrm{M}}(a/a_{\mathrm{M}})$ and $\varepsilon_{\mathrm{S}} = \varepsilon_{\mathrm{S}}(a/a_{\mathrm{S}})$.

[7]Explicit expressions for $h_{\boldsymbol{n}}$ for each of the 29 distinct curves of secular resonances are given in [11].

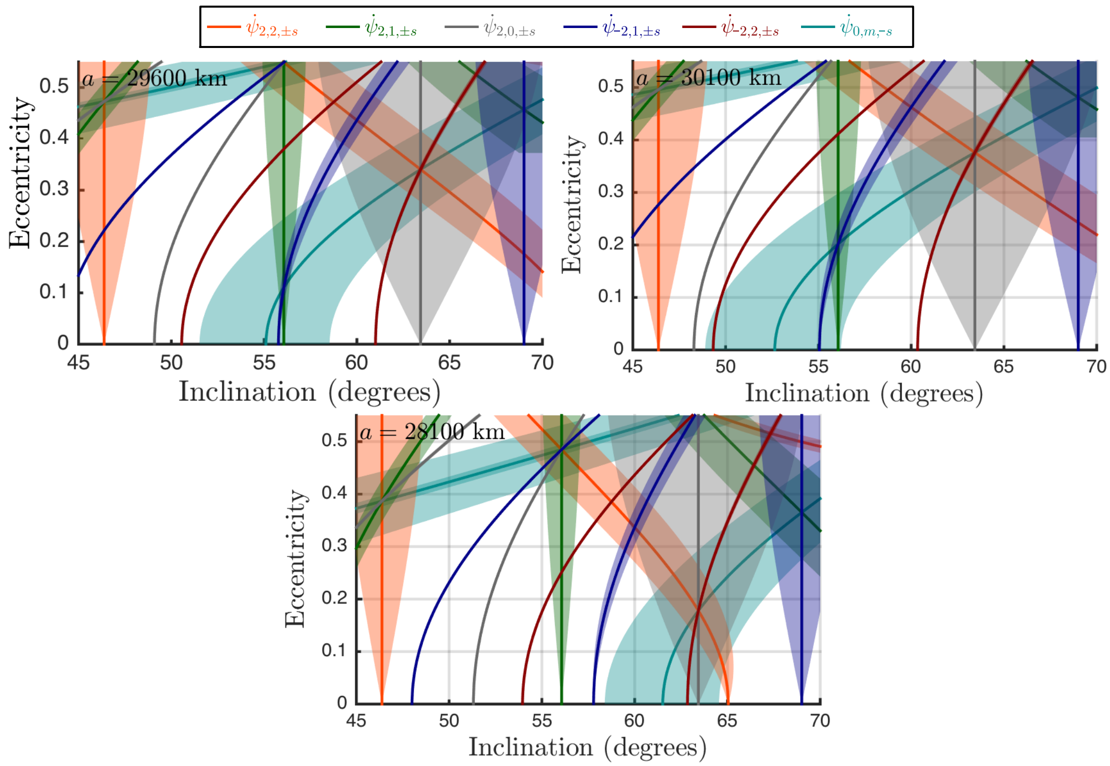

Figure 4. Lunisolar resonance centers $\mathscr{C}_{\boldsymbol{n}}$ (solid lines) and widths $\mathscr{W}_{\boldsymbol{n}}^{\pm}$ (transparent shapes) for various values of the satellite's semi-major axis near Galileo. This plot shows the regions of overlap between distinct resonant harmonics.

This basic understanding reached, using pen-and-paper calculations in the manner of Lagrange and Laplace, is a strong testimony to the enduring power of analytical theories in celestial mechanics.

Figure 4 gives the basic regions in the 2D inclination–eccentricity phase space for which chaotic orbits can be found, but gives no information about which initial angles (ω, Ω, and Ω_M) will lead to chaos. For this, we turn to the numerical detection of chaotic and regular motion through FLI stability and Lyapunov time maps, which furthermore provide a global visualization of the curious symbiosis of these two fundamental types of behaviors.

4. FLI Stability Analysis

It was shown in [11] that model 1 in Tab. 1 captures, qualitatively and quantitatively, all of the dynamical structures revealed by the more realistic and more complicated models. We cannot show here how abundant and fruitful the consequences of this realization have proved. The application of this basic physical model leads to simple and convincing explanations of many facts previously incoherent and misunderstood. Here we tailor the recent results of [11], to which we refer for omitted details, to the evaluation of the proposed disposal strategies.

Figures 5 and 6 present several dynamical quantities of interests, in a series of maps[8], for semi-major

[8] To produce the various stability maps, the initial conditions were distributed in a regular grid of 200×200 resolution,

axes and parameters near the disposal orbits of Section 2.: the FLIs [19, 20], characterizing the degree of hyperbolicity; the Lyapunov time, an estimate of the prediction horizon; and collision time. The FLIs of all regular orbits appear with the same dark blue color, while light blue corresponds to invariant tori, yellow and red to chaotic regions, and white to collision orbits. We find that the volume of collision orbits is roughly the same for the stable and unstable semi-major axes, but that the volume of chaotic obits is indeed larger for the eccentricity growth scenario (where we also find highly unstable and re-entry orbits even for quasi circular orbits). Inside the collision orbit structures, the re-entry time is nearly constant, and the shortest dynamical lifetime was almost identical in both cases (~ 120 years). For each scenario, the values of the estimated Lyapunov times imply a very short timescale for reliable predictability, with many orbits having values on the order of a few decades.

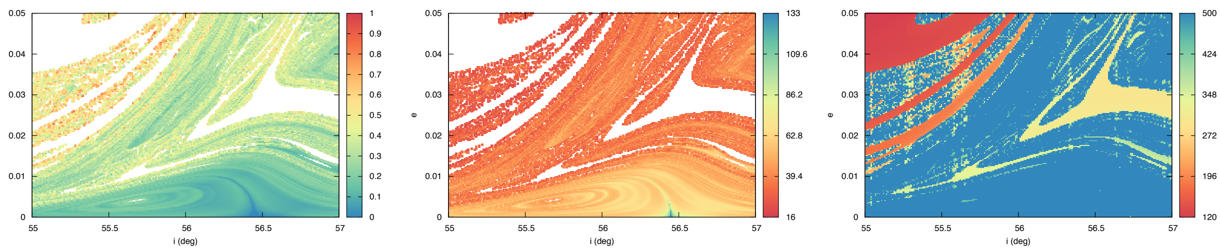

(a) FLI map. (b) Lyapunov time map. (c) Collision time map.

Figure 5. Stability maps characterizing the local hyperbolicity and the barrier of predictability in the vicinity of a proposed graveyard orbit case ($a_0 = 30,100$ km, $\Omega_0 = \omega_0 = 70°$, epoch: 6 DEC 2020). The collision time map is provided to illustrate the period of time after which atmospheric re-entry occurs, and completes the variational maps.

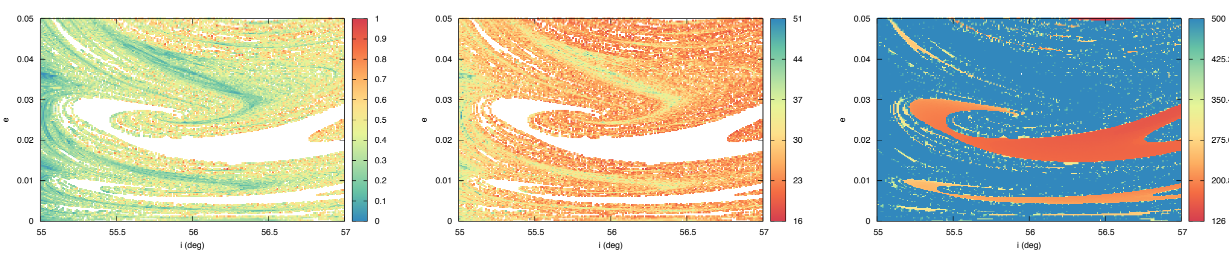

(a) FLI map. (b) Lyapunov time map. (c) Collision time map.

Figure 6. Same as Fig. 5, but for a proposed eccentricity growth case ($a_0 = 28,100$ km, $\Omega_0 = 60°$, $\omega_0 = 100°$, epoch: 6 DEC 2020).

We must stress here that all of these charts, Figs. 5 and 6, have been obtained by varying only the initial inclination and eccentricity, with the initial phases (t_0, Ω, ω) being fixed for all computed FLI. Given the inherent difficulty to capture the dynamics of the whole six-dimensional phase space in a plane of dimension two, we must settle for only a partial insight into the dynamical structure [20, 21]. We now fix the action-like quantities to their approximate nominal values, along with the epoch date, and investigate the geometrical organization and coexistence of chaotic and regular motion in the Ω–ω phase space (Fig. 7). Note the similarity between the MEM maps of Fig. 1 (top),

and the model was propagated for 500 years.

computed over a 200 year timespan; yet, the FLI and Lyapunov time maps, besides providing much finer detail for the proper detection of invariant structures and chaotic regions, give actual physical information on these unpredictable orbits, whereas the MEM maps provide only one trajectory realization. In the stable case, we point out again how the structures seem to be aligned along vertical bands, and can observe a highly stable region near $\Omega = 210^\circ$ (notice how the misleadingly wide bands of stable orbits in Fig. 1 disappear in a proper resolution and computational time). The volume of escaping orbits is larger for the unstable case, and it becomes much more difficult to identify stable regimes.

Figure 8 presents the evolution of the FLI maps in the node–perigee phase space, exploring the sensitivity to the initial semi-major axis near the nominal Galileo value. It is particularly noteworthy that the volume of stable orbits is found to increase with increasing semi-major axis, as with the width of the vertical band of stability, occurring near $\Omega = 180^\circ$. The location of this strip of stability is related to the resonant geography of the observed area (Fig. 4), and an analytical description of these structures will be pursued in a future work. On the contrary, decreasing the initial semi-major axis from the Galileo constellation (where the precise identification of stability pockets already presents a difficult task), the Ω–ω phase-space is nearly globally populated by unstable orbits that surround collisions orbits, the latter organized in pendulum-like structures.

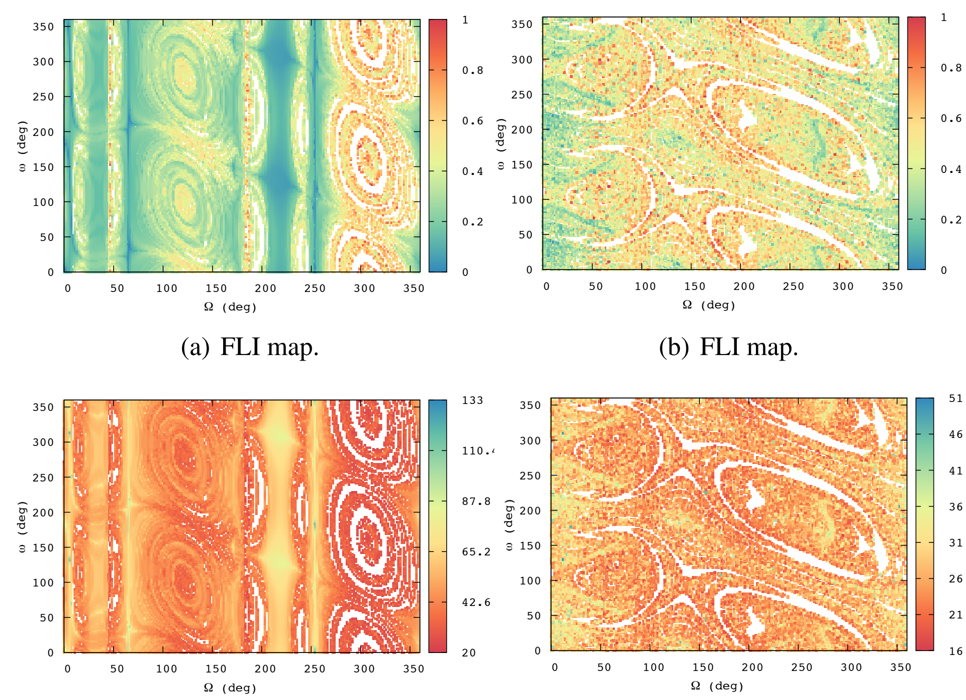

(a) FLI map. (b) FLI map.

(c) Lyapunov time map. (d) Lyapunov time map.

Figure 7. Dynamical structures of the stable (left: $a_0 = 30,100$ km, $e_0 = 0.001$, $i_0 = 56^\circ$) and unstable (right: $a_0 = 28,100$ km, $e_0 = 0.05$, $i_0 = 56^\circ$) cases in the node–perigee phase space.

Figure 9 shows how the dynamical structures (stable, resonant, chaotic, or collision orbits) evolve by changing the initial phases Ω and ω or even the initial dynamical configuration of the Earth-Moon-Sun system (equivalent to changing the initial epoch). Of course, the FLI maps depend on the choice of initial angles because, as Todorović and Novaković write, "… planes fixed at their different

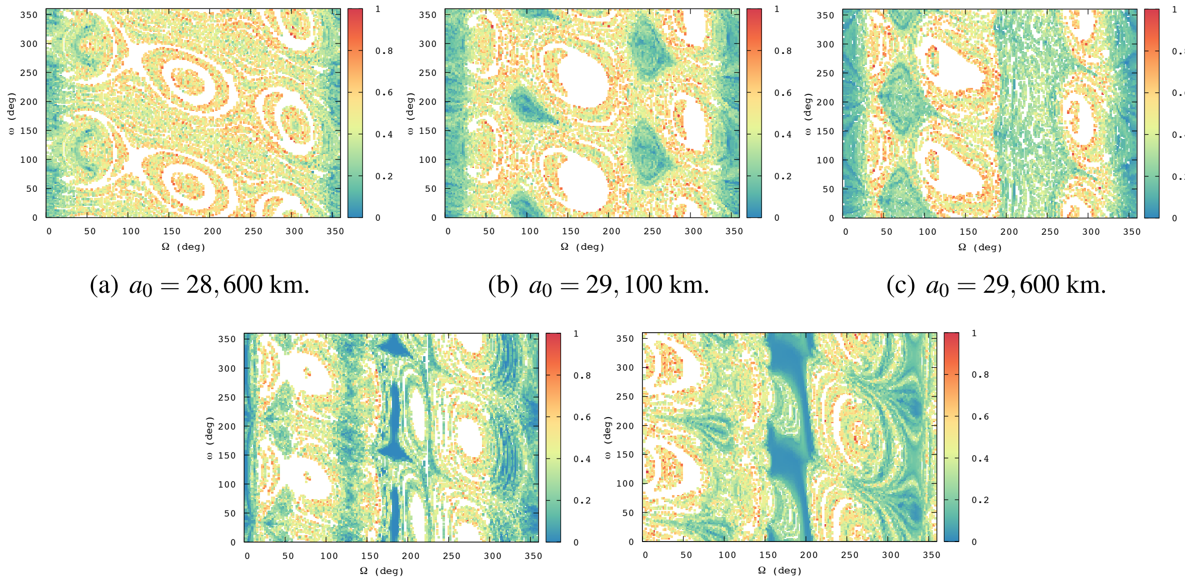

(a) $a_0 = 28,600$ km. (b) $a_0 = 29,100$ km. (c) $a_0 = 29,600$ km.

(d) $a_0 = 30,100$ km. (e) $a_0 = 30,600$ km.

Figure 8. Influence of the strength of the perturbation on the dynamical structures near Galileo's semi-major axis ($e_0 = 0.02$, $i_0 = 56.1^\circ$, epoch: 2 MAR 1969).

values cross the resonant islands at different positions, and in some special cases the crossing may not even occur. After all, the orbital space is 6D, while our plots are 2D, which certainly gives only a partial insight into the phase-space structure. However, we underline that this does not change the global dynamical pictures of the region, which is essential the same ... [20]". To understand how such features evolve is clearly of remarkable practical application, and will require further study.

5. Conclusion

It is no longer possible to investigate the motion of celestial bodies without being fully conscious of the possibilities of chaos, a fact well known to dynamical astronomers but seemingly oblivious to space engineers. Resonant and chaotic phenomena are ubiquitous in multi-frequency systems, and the knowledge of their long-period effects is essential for determining the stability of orbits and the lifetime of satellites. The complexity of the dynamical environment occupied by the Earth's navigation satellites is now becoming clearer [12, 11]. Resonant phenomena are widespread within the medium-Earth orbit (MEO) region as a whole, but particularly so amongst the highly inclined orbits of the navigation satellite systems, and a clear picture of the dynamics near these resonances is of considerable practical interest. We can now identify the sources of orbital instability or their absence in the MEO region and their nature and consequences in the context of long-term dynamical evolution. We examined them in terms of the detection of stability and unstable zones, with a particular view on the choice of the Galileo constellation disposal orbits. This paper links theoretical aspects of resonant and chaotic dynamics with practical applications, and lays an essential logical foundation for future developments.

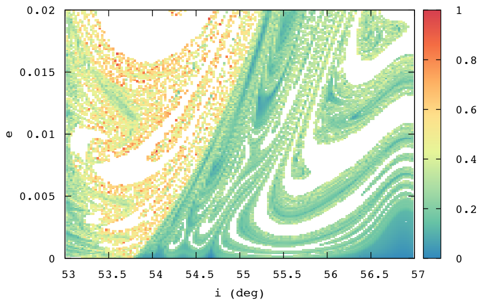

(a) $\Omega = 240°$, $\omega = 30°$, epoch: 2 MAR 1969.

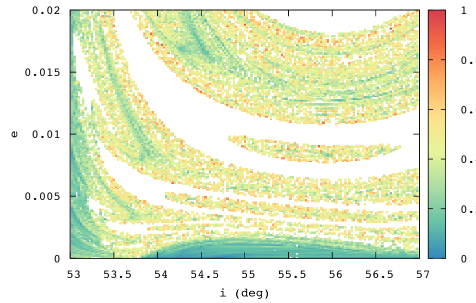

(b) $\Omega = 120°$, $\omega = 120°$, epoch: 2 MAR 1969.

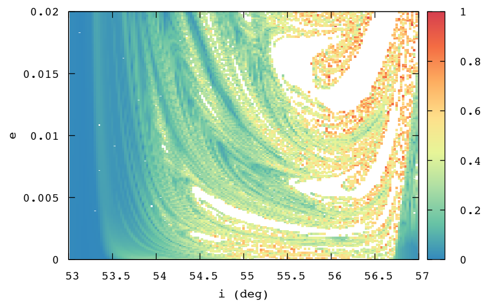

(c) $\Omega = 120°$, $\omega = 120°$, epoch: 23 AUG 1974.

Figure 9. Influence of the initial phases and the initial configuration of the Earth-Moon-Sun system in the representation of a dynamical system in a lower dimensional phase space.

6. Acknowledgements

We thank Fabien Gachet and Ioannis Gkolias, of the University of Rome Tor Vergata, for their technical contributions to this paper and for motivating conversations. This work is partially funded by the European Commissions Framework Programme 7, through the Stardust Marie Curie Initial Training Network, FP7-PEOPLE-2012-ITN, Grant Agreement 317185. Part of this work was performed in the framework of the ESA Contract No. 4000107201/12/F/MOS "Disposal Strategies Analysis for MEO Orbits".

7. References

[1] Morbidelli, A. Modern Celestial Mechanics: Aspects of Solar System Dynamics. Taylor & Francis, London, 2002.

[2] Zeebe, R. E. "Highly stable evolution of Earth's future orbit despite chaotic behavior of the Solar System." Astrophys. J., Vol. 811, 2015. Art. ID 9.

[3] Barrow, J. D. "Simple really: from simplicity to complexity – and back again." B. Bryson, editor, "Seeing Further: The Story of Science, Discovery, and the Genius of the Royal Society," pp. 360–383. Harper Press, London, 2010.

[4] Lichtenberg, A. J. and Lieberman, M. A. Regular and Chaotic Dynamics. Springer-Verlag, New York, 2 edn., 1992.

[5] Laskar, J. and Gastineau, M. “Existence of collisional trajectories of Mercury, Mars and Venus with the Earth.” Nature, Vol. 495, pp. 817–819, 2009.

[6] Brouwer, D. “Solution of the problem of artificial satellite theory without drag.” Astron. J., Vol. 64, pp. 378–397, 1959.

[7] Alessi, E. M., Rossi, A., Valsecchi, G. B., Anselmo, L., Pardini, C., Colombo, C., Lewis, H. G., Daquin, J., Deleflie, F., Vasile, M., Zuiani, F., and Merz, K. “Effectiveness of GNSS disposal strategies.” Acta Astronaut., Vol. 99, pp. 292–302, 2014.

[8] Radtke, J., Sven, K., Sanchez-Ortiz, N., Dominguez-Gonzalez, R., and Merz, K. “Impact of eccentricity build-up and graveyard disposal strategies on MEO Navigation Constellations.” “Proc. 40th COSPAR Scientific Assembly (COSMOS, Moscow, Russia, August 2014),” Paper PEDAS.1-23-14. 2014.

[9] Sanchez, D. M., Yokoyama, T., and Prado, A. F. B. A. “Study of some strategies for disposal of the GNSS satellites.” Math. Probl. Eng., Vol. 2015, 2015. Art. ID 382340.

[10] Chao, C. C. “MEO disposal orbit stability and direct reentry strategy.” Adv. Astronaut. Sci., Vol. 105, pp. 817–838, 2000.

[11] Daquin, J., Rosengren, A. J., Alessi, E. M., Deleflie, F., Valsecchi, G. B., and Rossi, A. “The dynamical structure of the MEO region: long-term stability, chaos, and transport.”, 2015. ArXiv:1507.06170.

[12] Rosengren, A. J., Alessi, E. M., Rossi, A., and Valsecchi, G. B. “Chaos in navigation satellite orbits caused by the perturbed motion of the Moon.” Mon. Not. R. Astron. Soc., Vol. 449, pp. 3522–3526, 2015.

[13] Dvorak, R., Pilat-Lohinger, E., Funk, B., and Freistette, F. “Planets in habitable zones: A study of the binary Gamma Cephei.” Astron. Astrophys., Vol. 398, pp. L1–L4, 2003.

[14] Nagy, I., Süli, Á., and Érdi, B. “A stability study of Pluto’s moon system.” Mon. Not. R. Astron. Soc., Vol. 370, pp. L19–L23, 2006.

[15] Ramos, X. S., Correa-Otto, J. A., and Beaugé, C. “The resonance overlap and Hill stability criteria revisited.” Celest. Mech. Dyn. Astr., 2015. doi:10.1007/s10569-015-9646-z.

[16] Perozzi, E., Roy, A. E., Steves, B. A., and Valsecchi, G. B. “Significant high number of commensurabilities in the main lunar problem. I: The Saros as a near-periodicity of the Moon’s orbit.” Celest. Mech. Dyn. Astr., Vol. 52, pp. 241–261, 1991.

[17] Musen, P. “On the long-period lunar and solar effects on the motion of an artificial satellite, 2.” J. Geophys. Res., Vol. 66, pp. 2797–2805, 1961.

[18] Wisdom, J. “Canonical solution of the two critical argument problem.” Celest. Mech., Vol. 38, pp. 175–180, 1986.

[19] Froeschlé, C., Guzzo, M., and Lega, E. “Graphical evolution of the Arnold web: From order to chaos.” Science, Vol. 289, pp. 2108–2110, 2000.

[20] Todorović, N. and Novaković, B. "Testing the FLI in the region of the Pallas asteroid family." Mon. Not. R. Astron. Soc., Vol. 451, pp. 1637–1648, 2015.

[21] Richter, M., Lange, S., Bäcker, A., and Ketzmerick, R. "Visualization and comparison of classical structures and quantum states of four-dimensional maps." Phys. Rev. E, Vol. 89, 2014. Art. ID 022902.